Available online at www.sciencedirect.com
ScienceDirect
Journal of Molecular Catalysis A: Chemical 270 (2007) 93–100
JOURNAL OF MOLECULAR CATALYSIS A: CHEMICAL
www.elsevier.com/locate/molcata

Carbon-containing nano-titania prepared by chemical vapor deposition and its visible-light-responsive photocatalytic activity

Chien-Sheng Kuo [a], Yao-Hsuan Tseng [b], Chia-Hung Huang [b], Yuan-Yao Li [a,*]

[a] *Department of Chemical Engineering, National Chung-Cheng University, Chia-Yi 621, Taiwan*
[b] *Energy and Environment Research Laboratories, Industrial Technology Research Institute, Hsinchu 310, Taiwan*

Received 19 July 2006; received in revised form 11 January 2007; accepted 14 January 2007
Available online 24 January 2007

Abstract

Ultraviolet and visible-light-responsive titania was synthesized and employed in the NO_x photomineralization. A thermal decomposition reaction of titanium isopropoxide was carried out with a metal-organic chemical vapor deposition (MOCVD), enabling continuous production of TiO_2 nanoparticles. Carbon-containing titanium dioxide with the anatase phase prepared at 500 °C under nitrogen atmosphere exhibited high photocatalytic activity for NO oxidation under visible-light illumination. Experimental results indicate that up to 48% removal of NO_x can be achieved in a continuous flow type of reaction system under visible-light illumination (green LED). The chamber temperature in this MOCVD process plays an important role in lattice structure formation, and also affected TiO_2 carbon content. The carbonaceous species on the TiO_2 surface, shown by X-ray diffractometry (XRD), and Raman, UV–vis, and X-ray photoelectron spectroscopies (XPS), is important to the visible-light absorption and visible-light-catalytic mineralization of NO_x.

Keywords: Visible-light-responsive photocatalyst; Carbon-containing; Chemical vapor deposition

1. Introduction

Since the discovery of photoelectrochemical water splitting using titanium dioxide electrodes [1], researchers have extensively studied semiconductor-based photocatalysis. Today, titanium dioxide is the most common photocatalyst material due to its strong redox ability and wide use in air purification, water treatment, deodorization, self-cleaning, sterilization coating [1–4], and other applications. In environmental applications, TiO_2 exhibits excellent photocatalytic abilities for mineralizing NO_x, SO_x, and VOCs under solar irradiation. TiO_2 absorbs photons, and evolves active oxygen species, such as OH radicals and O_2^- ions, by reacting with H_2O and O_2 adsorbed on the TiO_2 surface. The high oxidation potential of active oxygen species decomposes many kinds of pollutants [3–5].

Many photocatalytic applications use nano-sized anatase phase TiO_2. A light source shorter than 388 nm in wavelength can activate a TiO_2 photocatalyst with an energy gap of 3.2 eV. Approximately 4% of the energy in the solar light spectrum on the earth's surface comes from the 280 to 400 nm wavelength UV region. Meanwhile, the 400–700 nm wavelength visible-light region accounts for 45% of the energy. Further, UV light intensity, 0.1–5 $\mu W/cm^2$, is very low in indoor illumination. This has limited TiO_2 applications, giving visible-light-responsive photocatalysts much more attention for increasing solar and indoor lighting energy utilization. Previous studies considered the sol–gel method [6], sputtering plasma [7,8], and metal ion-implantation [9,10] to enhance the visible-light response of TiO_2. However, the equipment required for these methods is expensive, and mass production is difficult. Materials such as CdS, TaN_5, TaON, and $InVO_4$ [11,12] also function as visible-light-responsive photocatalysts. Photocatalytic water splitting researchers have studied and developed these methods and materials. However, environmental purification requires considering the cost and stability of a material for any practical application. Few feasibility studies exist for these methods and materials for industrial-scale production due to their higher cost, environment pollution issues, and material instability. A metal-organic chemical vapor deposition (MOCVD) is a practical way to produce visible-light-responsive TiO_2 material because it enables

* Corresponding author.
E-mail address: chmyyl@ccu.edu.tw (Y.-Y. Li).

1381-1169/$ – see front matter © 2007 Elsevier B.V. All rights reserved.
doi:10.1016/j.molcata.2007.01.031

the mass production of high quality nanoparticles as well as thin films [13–15]. This process also controls photocatalyst influential factors such as composition, crystal structure, purity, and particle size [15–17].

This study aims to prepare TiO_2 nanoparticles with large surface areas, narrow particle size distribution, and high visible-light-responsive activity. Specifically, this paper reports the thermal decomposition reaction of titanium isopropoxide (TTIP) to synthesize photocatalyst particles by the MOCVD method at various growth temperatures. Synthesized nanoparticles were collected at the reactor outlet via thermophoretic collection [18]. The synthesized photocatalysts were then evaluated for NO_x degradation under visible-light illumination. This study also carried out various characterization analyses of the visible-light-responsive TiO_2 to determine the crystal phase, particle size, UV–vis absorption, and surface composition.

2. Experimental

2.1. Apparatus, experimental conditions and characterization

Fig. 1 shows a diagram of the experimental setup, which was reported in a previous study [15]. This setup consists of stainless steel gas flow lines, mass flow controllers, a syringe pump, and a quartz tube (25 mm o.d., 23 mm i.d., and 1000 mm long) in an electric furnace functioning as the reactor. The hot zone was 300 mm long. A mass flow controller and a syringe pump controlled the gas and titanium isopropoxide flow rates, respectively. A mechanical pump enabled a low pressure operation, to a few Torr, and a convectron gauge measured the chamber pressure. A stainless steel net trapped the product in a collection system assembled with a 4 °C cooling jacket, which reduced particle aggregation.

The quartz tube was purged by nitrogen during the initial heating step. Upon reaching the desired reaction temperature (between 400 and 1000 °C), the furnace reactor was filled with a mixture of TTIP (1.0 mL/min) as the catalyst precursor and nitrogen (500 sccm) as the carrier gas. Oxygen gas was also introduced at 100 sccm, as necessary. The collection system gathered the resulting TiO_2 powder. After a 10 min reaction, the reactor returned to room temperature under a 100 sccm nitrogen flow. The synthesized TiO_2 materials was named TiO_2_X when prepared in the MOCVD process under a nitrogen atmosphere at X °C. If the photocatalysts were prepared in the presence of oxygen gas, the sample was named TiO_2_X(O).

The photocatalyst crystal phase was identified using X-ray diffractometry with Cu Kα radiation (Shimadzu XRD 6000). Material compositions were determined by X-ray photoelectron spectroscopy (Perkin Elmer SSI-M probe XPS system). Measuring average particle size and morphology was performed by transmission electron microscopy (TEM, Hitachi S600-100KV). The surface area of the powders was measured by nitrogen adsorption using the BET equation (Micrometrics Model ASAP 2400). Ultraviolet–visible light absorption spectra were obtained with a powder spectrophotometer (Shimadzu UV-2450). Photocatalyst surface structures were identified by a Raman spectrometer (Renishaw 1000B), and a scattering experiment was conducted with a low-power green laser (30 mW) at 532 nm for 10 s.

2.2. NO_x degradation over TiO_2 photocatalyst

Fig. 2 depicts the continuous flow system where NO_x degradation was performed. A round-shaped Pyrex glass vessel was used to conduct the NO_x, and a sample dish was located inside the vessel containing the TiO_2 powder. LEDs (visible light) or a black lamp (UVA light) provided a light source with an intensity of 1 mW/cm^2. The light source spectra, shown in Fig. 3, were measured using a spectrophotometer (Ocean Optics, USB2000). The NO_x degradation was carried out at room temperature using an air stream containing 1.0 ppm NO as feedstock. Two mass flow controllers (MFCs) (Brooks 5850E) manipulated relative humidity in the feeding stream. The reaction gas in the feeding stream passed through the vessel containing TiO_2 powder (0.2 g) at a flow rate of 1 L/min. An on-line chemiluminescent NO_x analyzer (Eco Physics, CLD 700 AL) continuously monitored NO and NO_2 concentrations for gas analysis in the outlet.

3. Results and discussion

3.1. Photocatalyst activity under UV- and visible-light irradiation

Many researchers use NO oxidation to determine photocatalytic reactivity in various TiO_2 photocatalytic applications [19–24]. The electron–hole pair (e^-–h^+) generated upon light

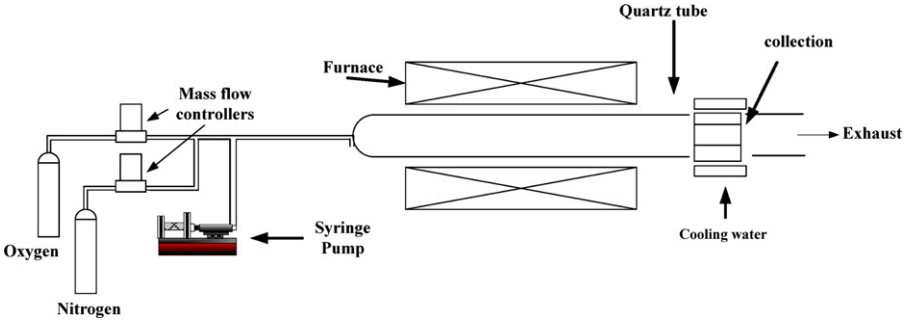

Fig. 1. Schematic diagram of the TiO_2 synthesis reactor.

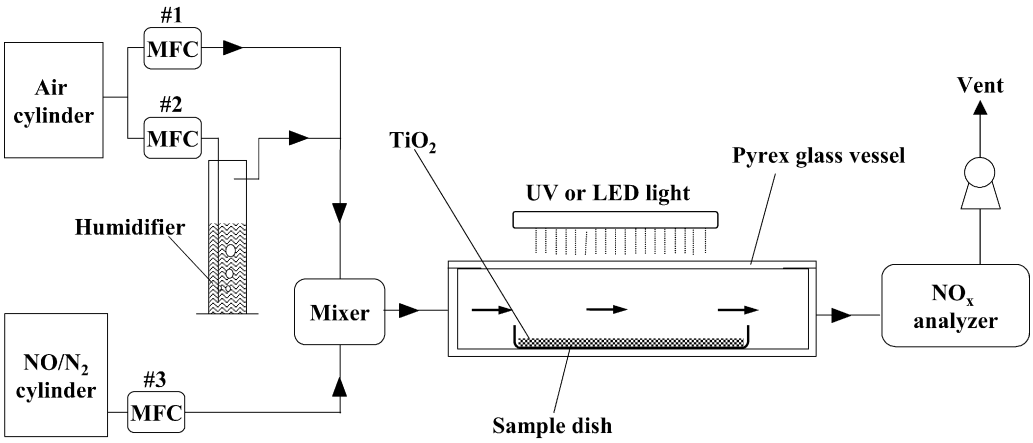

Fig. 2. Schematic diagram of continuous flow system for photocatalytic NO_x removal.

excitation is trapped at the TiO_2 surface as spatially separated redox active sites. Some studies report the formation of reactive oxygen species, such as superoxide ion ($O_2^{\bullet -}$), atomic oxygen (O), O^-, OH and HO_2 radicals on the surface of TiO_2 irradiated with UV light [25–27]. The general mechanism of NO_x oxidation by photocatalyst is as follows. Hydrogen ions and hydroxide ions are dissociated from water. The active oxygen species are produced on the TiO_2 surface.

$$O_2 + e^- \rightarrow O_2^- \quad (1)$$

$$OH^- + h^+ \rightarrow OH^* \quad (2)$$

$$H^+ + O_2^- \rightarrow HO_2^* \quad (3)$$

The nitric monoxide is oxidized to nitric acid or nitrous acid by active oxygen species. Based on the gas-phase chemistry of NO_x [28], NO is converted to HNO_3 as a consecutive photooxidation via a NO_2 intermediate.

$$NO + HO_2^* \rightarrow NO_2 + OH^* \quad (4)$$

$$NO_2 + OH^* \rightarrow HNO_3 \quad (5)$$

$$NO + OH^* \rightarrow HNO_2 \quad (6)$$

Finally, the nitric acid forms on the catalyst. Photocatalyst activity lessens as acid accumulates. To illustrate the reaction behavior of NO photocatalytic oxidation, 0.2 g of TiO_2_500 and 1 mW/cm^2 of light intensity were used to conduct the experiment. Fig. 4 shows the NO_x oxidation results under UVA and visible light performed in a continuous flow system. At first, a 1 ppm NO gas stream was introduced into the reactor under dark conditions. The NO concentration in the gas phase dropped due to NO adsorption on the TiO_2. A few minutes later, the NO was saturated on the TiO_2, and the NO concentration was returned to 1 ppm. As Fig. 4 shows, the steady state of this photocatalytic reaction was achieved as soon as the photocatalyst was illuminated. The NO concentration decreased from 1 to 0.46 ppm, and the NO_2 concentration increased to 0.06 ppm. The NO_x concentration, which includes NO and NO_2 concentrations, was maintained at 0.52 ppm for 30 min under green LED illumination. TiO_2_500 activity did not obviously decrease

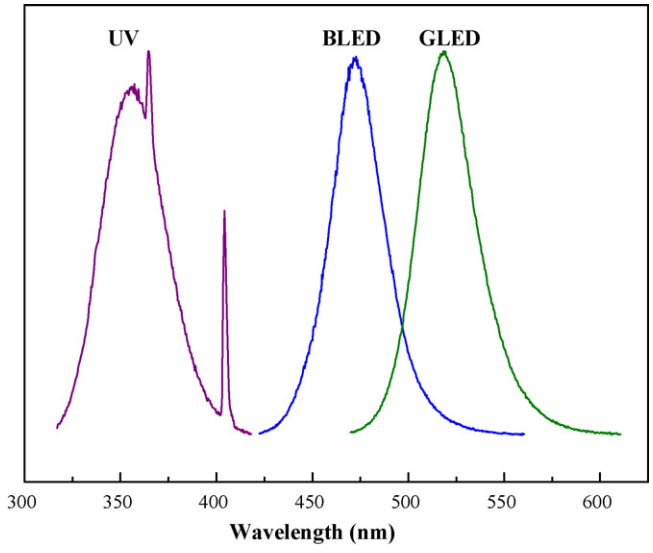

Fig. 3. UVA lamp and LED photon energy distribution profiles (the visible-light region of UVA lamp is small and not shown in this figure).

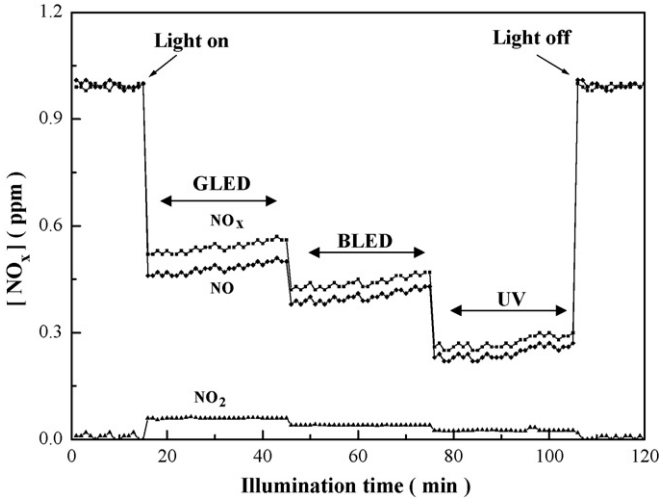

Fig. 4. Reaction profiles of NO over the TiO_2_500 photocatalyst during 1.5 h on stream; catalyst loading: 0.2 g; intensity of irradiation: 1 mW/cm^2; inlet concentration of NO: 1 ppm; inlet flow rate: 1 L/min; reaction temperature: 27 °C.

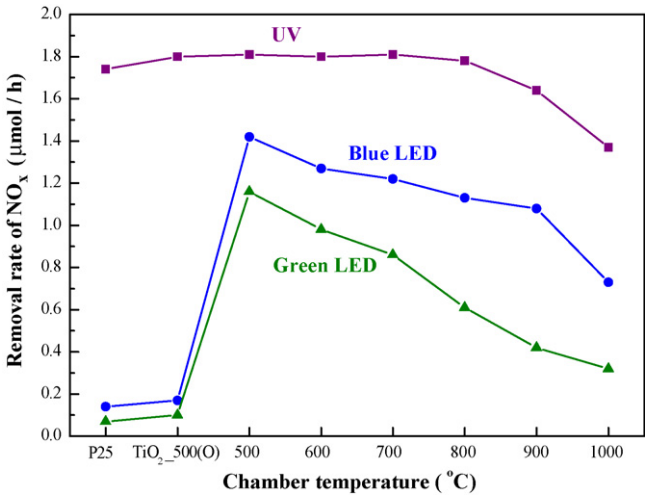

Fig. 5. Average removal rate of NO_x (μmol/h) on various photocatalysts vs. wavelength of irradiation; catalyst loading: 0.2 g; irradiation intensity: 1 mW/cm^2; inlet concentration of NO: 1 ppm; inlet flow rate: 1 L/min; reaction temperature: 27 °C.

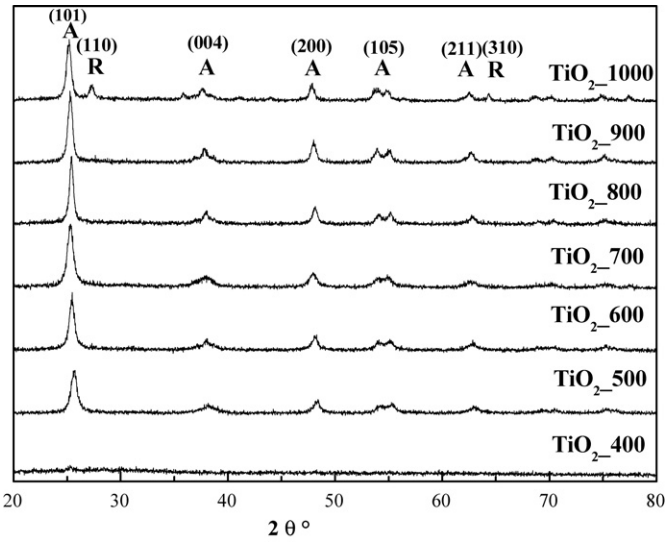

Fig. 6. XRD patterns of prepared photocatalysts.

over time, probably due to a large surface area of 109 m^2/g. Under a blue LED, NO, NO_2, and NO_x concentrations decreased to 0.38, 0.04, and 0.42 ppm, respectively. The amount of NO_x removal increased as the illumination wavelength decreased, but the amount of NO_2 generated increased as the illumination wavelength increased. This is because the number of induced active sites on the TiO_2 surface decreased with the increase in the wavelength of illumination, and NO_2 is more difficult to oxidize than NO. Hence, the decreasing reaction rate under visible light is primarily caused by the decrease in the NO_2 oxidation rate.

The comparison above used commercially available photocatalysts (Degussa P25). Fig. 5 shows NO_x removal rates using various photocatalysts under UV- and visible-light irradiation. Under UV illumination, these photocatalysts exhibit a similar activity in NO_x mineralization, except for TiO_2_900 and TiO_2_1000. TiO_2_400 was inactive. Although the photoactivities of P25 and TiO_2_500(O) were good under UV illumination, their visible-light activities were low. These results demonstrate that the activity of prepared TiO_2 decreases as the synthesis temperature increases. Under visible light, the activity levels of these photocatalysts fell in the order of TiO_2_500 > TiO_2_600 > TiO_2_700 > TiO_2_800 > TiO_2_900 > TiO_2_1000–TiO_2_500(O) > P25. This order of activity is the same under different visible-light sources (blue and green lights). Adding oxygen gas to the synthesis reaction obviously decreased the visible-light response of prepared TiO_2. Therefore, the optimal CVD reaction temperature is 500 °C, without adding oxygen gas, for the highest visible-light-responsive activity.

3.2. TiO_2 photocatalyst characterization

3.2.1. XRD

Fig. 6 shows the X-ray diffraction patterns of TiO_2 samples. At a synthesis temperature of 400 °C, no detectable peaks indicate the presence of an amorphous structure. This lack is responsible for the very low photocatalytic activity of TiO_2_400. The peaks for the (1 0 1), (0 0 4), (2 0 0), (1 0 5), and (2 1 1) reflections characteristic of the TiO_2 anatase phase appeared on the material at a synthesis temperature above 500 °C. Process temperatures ranging from 500 to 900 °C produce the anatase phase. The anatase phase was partially transformed to the rutile phase at 1000 °C [29]. The TiO_2 anatase phase is more photoactive than the rutile and brookite phases [30]. Sclafani and Hermann report that titania samples with the rutile phase were consistently much less photoactive than anatase samples [31]. Therefore, it was strongly suggested the synthesis temperature should not exceed 1000 °C due to the appearance of the rutile phase. The crystallite sizes of the prepared photocatalysts were determined from a half width of (1 0 1) peak using the Scherrer formula ($d = 0.9\lambda/\beta\cos\theta$). As shown in Table 1, vapor molecule accretion caused the crystallite size of TiO_2 to gradually increase as the temperature increased. Cluster–cluster and particle–particle collided rapidly, accelerating crystallite growth size (primary particle) and cluster (secondary particle) [32]. Porter et al. reports that crystallite size of sol–gel-synthesized TiO_2 and P25 rapidly increased over 700 °C [33]. However, the crystallite size of MOCVD-synthesized TiO_2 did not obviously increase with the temperature, and the rutile phase began to appear at a very

Table 1
Characterization of prepared TiO_2

Sample	C content (at.%)	Surface area (m^2/g)	Particle size (nm)[a]	Crystallite size (nm)[b]
TiO_2_500	22.2	109.4	14.1	9.8
TiO_2_600	20.4	61.0	25.3	10.6
TiO_2_700	17.7	58.9	26.2	11.2
TiO_2_800	16.5	41.6	37.1	13.5
TiO_2_900	14.2	29.0	53.1	15.9
TiO_2_1000	67.3	27.0	57.1	16.2
TiO_2_500(O)	5.63	138.3	11.2	7.7

[a] Calculated by BET formula, $d_{BET} = 6/\rho A$.
[b] Calculated by Scherrer formula, $d = 0.9\lambda/\beta\cos\theta$.

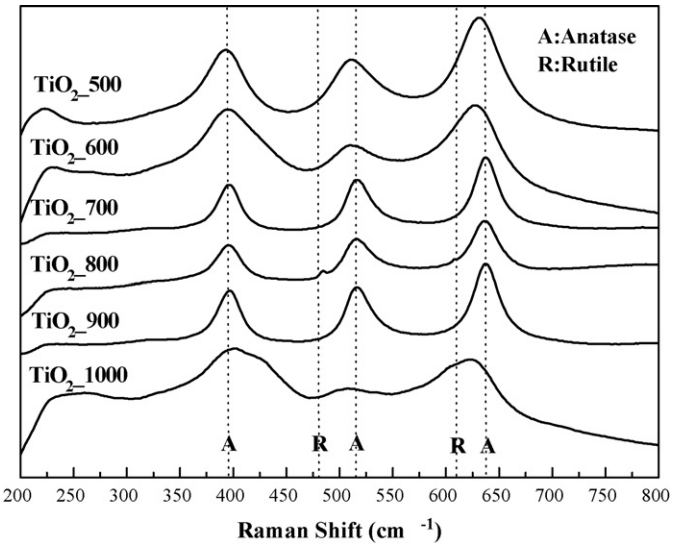

Fig. 7. Raman spectra of prepared photocatalysts.

high temperature (1000 °C). This is due to a short retention time (0.25 s) of TTIP in the heating zone during the synthesis process. The heat effect on crystallite size growth was not as obvious as in previous studies.

3.2.2. Raman spectroscopy

Raman spectroscopy can be used to clearly characterize the TiO_2 surface structure [20,34]. Raman spectroscopy wave vector selection rules, which limit the wave vector of detectable photons to the Brillouin zone center, break down at a very small size (>10 nm). As a result, all the spectra peaks broadened as the particle size decreased. Iida et al. [34] and Li et al. [35] both claim that this method is more sensitive for nanometer-sized crystals than X-ray diffraction. This study used lower laser power to avoid laser heating or laser damage effect. Fig. 7 shows TiO_2 Raman spectra at different synthesis temperatures. The Raman spectra were consistent with XRD patterns for TiO_2_500 to TiO_2_900. The anatase phase, Raman shift = 396, 517, and 638 cm^{-1} [36], existed in all TiO_2 samples, and the anatase phase peaks were narrowed with increasing synthesis temperature except for TiO_2_1000. This shows that the anatase crystallite size increased as the synthesis temperature increased from 500 to 900 °C. The broad and low blue-shift peaks of TiO_2_500 and TiO_2_600 were caused by a low degree of crystallization on the surface and small particles. The broad and weak intense peaks of TiO_2_1000 included both anatase and rutile phases, 440 and 608 cm^{-1}, due to the mixed and incomplete lattice structure (i.e., amorphous-like structure) on TiO_2 surface, which was not observed in the XRD pattern. The amorphous-like structure was probably caused by impurities such as carbonaceous species, covered or doped on the TiO_2 surface.

3.2.3. TEM

The morphology of the prepared photocatalysts was observed by TEM. Fig. 8 shows TEM images of TiO_2_500 and TiO_2_1000, where the mean particle sizes are close to 15 and 65 nm, respectively. The size distribution of TiO_2_500 particles was narrow and non-aggregated. In contrast, the sol–gel nanoparticle preparation method easily produced particle agglomeration after calcination at high temperature. The MOCVD process can produce a good visible-light-responsive TiO_2 without agglomeration under proper conditions. The particle sizes ranged from 10 to 70 nm, which increased as the reaction temperature increased. Morphological observation by TEM and XRD calculations reveal that the large particle size of TiO_2_1000 was mainly caused by agglomeration, not the growth of crystallite size.

3.2.4. BET

Table 1 shows the specific surface area of samples prepared by the BET method. Agglomeration caused the surface area to decrease as the synthesis temperature increased. Furthermore, TEM observation confirmed that the prepared TiO_2 powders had an almost spherical and nonporous form. Therefore, this relationship can be expressed by a simple equation, assuming a spherical and nonporous particle:

$$d_{BET} = \frac{6}{\rho A} \quad (7)$$

where d_{BET} is the calculated particle size (nm), ρ the density of TiO_2 (3.84 and 4.20 g/cm^3 for anatase and rutile, respectively), and A is the specific surface area (m^2/g) [37]. Table 1 shows that the calculated diameter of the particles is about 14–57 nm. The results of specific surface area agree well with the TEM observation, but were different from the XRD calculations. Yue

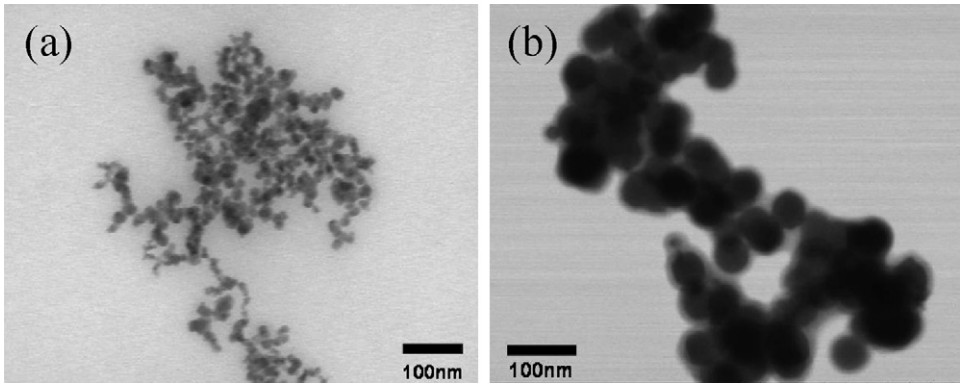

Fig. 8. TEM photograph of (a) TiO_2_500 and (b) TiO_2_1000.

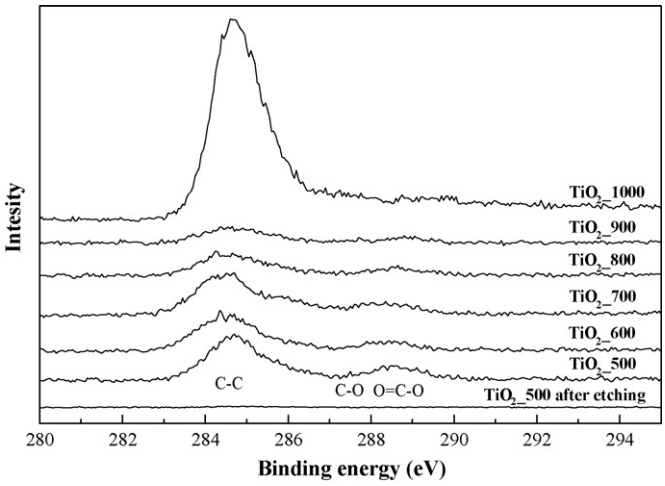

Fig. 9. C 1s XPS spectra of prepared photocatalysts.

and coworkers claim that the specific surface area of sol–gel-synthesized TiO_2 depends only on the size of crystals (primary particle) and was unaffected by aggregation [38]. This is probably because aggregation in the sol–gel process is loose, so the N_2 gas can penetrate the gap between aggregated particles. In this study, TiO_2 aggregation occurs mostly at high temperatures (>500 °C); therefore, the particles are tightly aggregated with high surface energy. Okuyama and coworkers report this phenomenon as incomplete sintering in the CVD process [16]. Hence, the specific surface area is more related to secondary particles than primary particles in this MOCVD process. Moreover, the specific surface area of TiO_2_500(O) was larger than all prepared samples due to a rapid nucleation rate in an oxygen atmosphere [39]. Nanoparticle size in the MOCVD process is determined by the relative magnitudes of nucleation and growth rate. The TTIP gas was totally decomposed to the monomer ($TiO_{2(g)}$), after which all monomers were converted into $TiO_{2(s)}$ in a very short time. This prevented further particle growth. Therefore, it is reasonable to assume that the grain size decreased after oxygen gas was added to the reaction atmosphere.

3.2.5. XPS

Some studies discuss carbon-doped and carbon-covered titania materials [19,20,40–46]. These researchers report that carbonaceous species play a sensitizer role, inducing visible-light absorption and response. To investigate the carbon states on the prepared TiO_2, the C 1s core levels were measured by XPS, as shown in Fig. 9. All samples were cleaned with irradiation of 2 mW/cm^2 UV light for 12 h before XPS analysis, removing the originally adsorbed organic compounds. Three XPS peaks occurred at 284.8, 286.7, and 288.8 eV for the prepared TiO_2. The first value arises from adventitious elemental carbon (C–C), and the other two small peaks indicate the existence of C–O and C=O, corresponding to a carbonate species [40,41]. The C–O and C=O were not chromophores, so the C–C structure on the TiO_2 surface is most likely responsible for visible-light absorption. The carbonaceous species covered the TiO_2 by the thermal decomposition reaction of TTIP. Without oxygen gas added to the reaction atmosphere, the TTIP alkoxide group was unable to completely convert to C_3H_6 and CO_2 gas. This caused the carbonaceous species, existing in the condensed and coke-like structure, to remain on the photocatalyst. Table 1 shows the carbon content in the TiO_2 at different synthesis temperatures. The amount of carbon on the TiO_2_500(O) is relatively low because the alkoxide group was completely oxidized to CO_2 gas in the presence of sufficient oxygen gas. The amount of carbon on the TiO_2 surface decreased as the synthesis temperature increased, except for the TiO_2_1000. The information from Fig. 5 and Table 1 indicates that the visible-light-responsive activity of prepared TiO_2 increased as the amount of carbon increased on the TiO_2, until 900 °C. The amount of carbon on the TiO_2 surface is responsible for good visible-light absorbance and visible-light-responsive activity. This finding agrees well with previous works by the same authors, and with Maier's experiment [19–21,45]. However, these visible-light-responsive TiO_2 samples were prepared in the CVD process under an anaerobic atmosphere, so a few oxygen atoms on the TiO_2 surface were substituted by carbon to form a $TiO_{2-x}C_x$ structure. The oxygen defects of TiO_2 possibly act as a recombination center, reducing photoactivity. XPS analysis of Ti $2p_{3/2}$ did not immediately reveal the Ti–C bond, so the $TiO_{2-x}C_x$ structure of these samples is probably scarce. In this case, the small number of oxygen defects in the TiO_2 samples does not enhance the recombination rate between excited electrons and holes, where the similar UV-responsive photoactivities of TiO_2_500(O) and TiO_2_500 samples obviously demonstrate this ratiocination, as shown in Fig. 5. The amount of carbon in the TiO_2_1000 material increased to 67%, but its UV- and visible-light-responsive activities were smaller than that of TiO_2_500 to TiO_2_900. TTIP thermal decomposition at an extremely high temperature caused this high amount of carbonaceous species. Many TTIP alkoxide groups transformed to highly condensed species, like coke, and were deposited and doped onto the TiO_2 surface. Thus, some photoactive sites were covered by coke species, causing an incomplete lattice structure (amorphous-like surface structure) on the TiO_2_1000 sample. This is shown in the Raman spectra. Therefore, the visible-light-responsive activity of TiO_2_1000 was less than TiO_2_500–900 in spite of its higher amount of carbonaceous species. In addition, after the Ar^+ ion etching process of TiO_2_500, the peak intensities of carbonaceous species decreased. After 120 s, carbon was not detected on the TiO_2. The etching experiment shows that the carbonaceous species mainly exist on the surface.

3.2.6. UV–vis diffuse reflectance spectra

Fig. 10 shows the UV–vis diffuse reflectance spectra of prepared TiO_2 materials and P25. This reflectance data was converted by instrument software to absorbance values, $F(R)$, based on the Kubelka–Munk theory [19,20,23,42,45]. The visible-light absorbance of the prepared TiO_2 depends on the synthesis temperature and the presence of oxygen gas. The visible-light absorption of these photocatalysts was in the order of TiO_2_1000 > TiO_2_500 > TiO_2_600 > TiO_2_700 > TiO_2_800 > TiO_2_900 > TiO_2_500(O)–P25. Except for TiO_2_1000, the order of visible-light-responsive activities was the same as the order of visible-light absorption. In this study, all photocatalysts prepared in an oxygen-free atmosphere exhibited much bet-

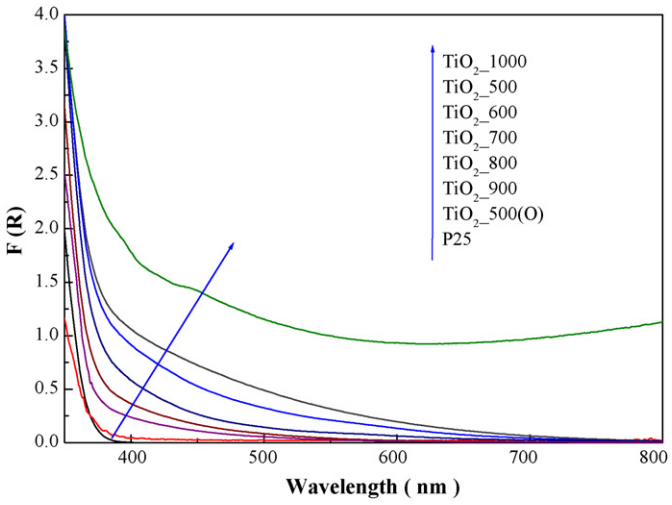

Fig. 10. UV–vis absorption spectra of various photocatalysts.

ter visible-light-responsive activities than commercial powder (P25). Furthermore, the TiO_2_500(O) sample, prepared in an oxygen atmosphere, and P25, did not perform well in visible-light absorption due to the absence of carbonaceous species. TiO_2_1000 possessed the highest visible-light absorption due to its huge amount of highly dense coke and amorphous-like surface structure. The visible-light absorptions of TiO_2_500 and TiO_2_600 were higher than others, except for TiO_2_1000. The amount of carbonaceous species on the surface of TiO_2_500 and TiO_2_600 was higher than on TiO_2_700, TiO_2_800, and TiO_2_900, but not very different. Raman analysis reveals a low crystallization on the surface of the TiO_2_500 and TiO_2_600, so the loose and amorphous-like structures of TiO_2_500 and TiO_2_600 were probably responsible for their better visible-light absorbance. In this experiment, TiO_2_700, TiO_2_800, and TiO_2_900 exhibited well-crystallized surface structures, so their visible-light absorbance was only due to the existence of carbonaceous species. Therefore, carbon in the samples may play two roles; it is the sensitizer for visible-light absorption due to its coke-like structure; and it also exists as an impurity, the lattice defect, of TiO_2 to form interface states that effectively lower the band gap.

4. Conclusions

Carbon-containing TiO_2 photocatalysts were successfully prepared by an MOCVD process using titanium isopropoxide as the precursor. Carbon-containing TiO_2 showed a relatively high photocatalytic activity in NO_x oxidation under visible-light illumination. The visible-light activity of prepared TiO_2 decreased as the synthesis temperature increased. The optimal synthesis temperature was 500 °C in an oxygen-free atmosphere. The coke-like carbonaceous species on the TiO_2 surface, as evidenced by XPS and Raman spectroscopy, are responsible for good visible-light absorption and photoactivity. The amount of TiO_2 carbonaceous species and visible-light response decreased as synthesis temperature increased, up to 900 °C. In conclusion, a simple and continuous process was achieved for preparing visible-light-responsive photocatalysts. These materials can be practically applied in the purification process in both water and air without UV illumination.

Acknowledgment

We thank the Ministry of Economic Affairs of the Republic of China, Taiwan, for financially supporting this research.

References

[1] A. Fujishima, K. Honda, Nature 238 (1972) 37.
[2] T. Ibusuki, K. Takeuchi, J. Mol. Catal. 88 (1994) 93.
[3] M.R. Hoffmann, S.T. Martin, W. Choi, D.W. Bahnemann, Chem. Rev. 95 (1995) 69.
[4] A. Fujishima, N.R. Tata, A.T. Donald, J. Photochem. Photobiol. C 1 (2000) 1.
[5] A. Mills, S.L. Hunte, J. Photochem. Photobiol. A 108 (1997) 1.
[6] T. Ohno, M. Akiyoshi, T. Umebayashi, K. Asai, T. Mitsui, M. Matsumura, Appl. Catal. A: Gen. 265 (2004) 115.
[7] R. Asahi, T. Morikawa, T. Ohwaki, K. Aoki, Y. Taga, Science 293 (2001) 269.
[8] I. Nakamura, N. Negishi, S. Kutsuna, T. Ihara, S. Sugihara, K. Takeuchi, J. Mol. Catal. A 161 (2000) 205.
[9] H. Yamashita, M. Harada, J. Misaka, M. Takeuchi, K. Ikeue, M. Anpo, J. Photochem. Photobiol. A 148 (2002) 257.
[10] M. Anpo, M. Takeuchi, K. Ikeue, S. Dohshi, Curr. Opin. Solid State Mater. 6 (2002) 381.
[11] G. Hitoki, A. Ishikawa, T. Takata, J.N. Kondo, M. Hara, K. Domen, Chem. Lett. 7 (2002) 736.
[12] G. Hitoki, T. Takata, J.N. Kondo, M. Hara, H. Kobayashi, K. Domen, Chem. Commun. 16 (2002) 1698.
[13] W. Li, S. Ismat Shah, M. Sung, C.P. Huang, J. Vac. Sci. Technol. B 20 (2002) 2302.
[14] S.C. Jung, S.J. Kim, N. Imaishi, Y.I. Cho, Appl. Catal. B: Environ. 55 (2005) 253.
[15] C.S. Kuo, Y.H. Tseng, Y.Y. Li, Chem. Lett. 35 (2006) 356.
[16] K. Nakaso, K. Okuyama, M. Shimada, S.E. Pratsinis, Chem. Eng. Sci. 58 (2003) 3327.
[17] O.J. Jung, S.H. Kim, K.H. Cheong, W. Li, S. Ismat Saha, Bull. Korean Chem. Soc. 24 (2003) 49.
[18] Y. Sun, T. Egawa, L. Zhang, X. Yao, Jpn. J. Appl. Phys. 41 (2002) 1389.
[19] Y.M. Lin, Y.H. Tseng, J.H. Huang, C.C. Chao, C.C. Chen, I. Wang, Environ. Sci. Technol. 40 (2006) 1616.
[20] Y.H. Tseng, C.S. Kuo, C.H. Huang, Y.Y. Li, P.W. Chou, C.L. Cheng, M.S. Wong, Nanotechnology 17 (2006) 2490.
[21] P.W. Chou, S. Treschev, P.H. Chung, C.L. Cheng, Y.H. Tseng, Y.J. Chen, M.S. Wong, Appl. Phys. Lett. 89 (2006) 131919.
[22] N. Negish, K. Takeuchi, T. Ibusuki, J. Mater. Sci. 33 (1998) 5789.
[23] T. Sano, N. Negishi, K. Koike, K. Takeuchi, S. Matsuzawa, J. Mater. Chem. 14 (2004) 380.
[24] S. Matsuda, H. Hatano, A. Tsutsumi, Chem. Eng. J. 82 (2001) 183.
[25] A. Walker, M. Formenti, P. Meriaudeau, S.J. Teichner, J. Catal. 50 (1977) 237.
[26] W.F. Behnke, F. Nolting, C. Zetzsch, J. Aerosol Sci. 18 (1987) 65.
[27] T. Ibusuki, K. Takeuchi, Atmos. Environ. 20 (1986) 1711.
[28] R. Atkinson, D.L. Baulch, R.A. Cox, R.F. Hampson Jr., J.A. Kerr, J. Troe, J. Phys. Chem. Ref. Data 18 (1989) 887.
[29] Y. Sun, T. Egawa, L. Zhang, X. Yao, Jpn. J. Appl. Phys. 41 (2002) 945.
[30] A. Masakazu, Y. Hiromi, I. Yuichi, E. Shaw, J. Electroanal. Chem. 396 (1995) 21.
[31] A. Sclafani, J.M. Herrmann, J. Phys. Chem. 100 (1996) 13655.
[32] Y. Sun, A. Li, M. Qi, L. Zhang, X. Yao, Mater. Sci. Eng. 86 (2001) 185.
[33] J.F. Porter, Y.G. Li, C.K. Chan, J. Mater. Sci. 34 (1999) 1523.

[34] Y. Iida, M. Furukawa, T. Aoki, T. Sakai, Appl. Spectrosc. 52 (1998) 673.
[35] M. Li, Z. Feng, G. Xiong, P. Ying, Q. Xin, C. Li, J. Phys. Chem. B 105 (2001) 8107.
[36] M.P. Moreta, R. Zallena, D.P. Vijayb, S.B. Desu, Thin Solid Films 366 (2000) 8.
[37] Y.H. Tseng, H.Y. Lin, C.S. Kuo, Y.Y. Li, C.P. Huang, React. Kinet. Catal. L 89 (2006) 63.
[38] A.J. Maira, K.L. Yeung, C.Y. Lee, P.L. Yue, C.K. Chan, J. Catal. 192 (2000) 185.
[39] Y. Sun, A. Li, M. Qi, L. Zhang, X. Yao, J. Mater. Sci. 37 (2002) 1343.
[40] M. Janus, B. Tryba, M. Inagaki, A.W. Morawaski, Appl. Catal. B: Environ. 52 (2004) 61.
[41] M. Inagaki, F. Kojin, B. Tryba, M. Toyoda, Carbon 43 (2005) 1652.
[42] S. Sakthivel, H. Kisch, Angew. Chem. Int. Ed. 42 (2003) 4908.
[43] Z. Jiang, C. Lu, H. Wu, Ind. Eng. Chem. Res. 44 (2005) 4165.
[44] T. Ohno, M. Akiyoshi, T. Umebayashi, K. Asai, T. Mitsui, M. Matsumura, Catal. Lett. 98 (2004) 255.
[45] C. Lettmann, K. Hildenbrand, H. Kisch, W. Macyk, W.F. Maier, Appl. Catal. B: Environ. 32 (2001) 215.
[46] S.U.M. Khan, M.W.B.I. Al-Shahry Jr., Science 297 (2002) 2243.